Optical Spectroscopic Investigation of the Alkaline Transition in Umecyanin from Horseradish Root†

Ines Delfino,‡ Katsuko Sato,§ Mark D. Harrison,§ Laura Andolfi,‡ Anna Rita Bizzarri,‡ Christopher Dennison,*,§ and Salvatore Cannistraro*,‡

Biophysics and Nanoscience Centre, INFM-CNISM, Dipartimento Scienze Ambientali, Università della Tuscia, Largo dell'Università, I-01100 Viterbo, Italy, and Institute for Cell and Molecular Biosciences, Medical School, University of Newcastle upon Tyne, Newcastle upon Tyne, NE2 4HH, United Kingdom

Received August 25, 2005; Revised Manuscript Received October 5, 2005

ABSTRACT: Umecyanin (UMC) from horseradish root belongs to the stellacyanin subclass of the phytocyanins, a family of plant cupredoxins. The protein possesses the typical type-1 His_2Cys equatorial ligand set at its mononuclear copper site but has an axial Gln ligand in place of the usual weakly coordinated Met of the plantacyanins, uclacyanins, and most other cupredoxins. UMC exhibits, like other phytocyanins, altered visible, EPR, and paramagnetic ^1H NMR spectra at elevated pH values and also a modified reduction potential. This alkaline transition occurs with a pK_a of ∼10 [Dennison, C., Lawler, A. T. (2001) *Biochemistry 40*, 3158−3166]. In this study, we investigate the alkaline transition by complementary optical spectroscopic techniques. The contemporary use of absorption, fluorescence, dynamic light scattering, and resonance Raman spectroscopy allows us to demonstrate that the alkaline transition induces a reorganization of the protein and that the overall size of UMC increases, but protein aggregation does not occur. The transition does not have a dramatic influence on the active-site environment of UMC, but there are subtle alterations in the Cu site geometry. Direct evidence for the strengthening of a Cu−N(His) bond is presented, which is in agreement with the hypothesis that the deprotonation of the $N^{\epsilon 2}H$ moiety of one of the His ligands is the cause of the alkaline transition. A weakening of the Cu−S(Cys) bond is also observed which, along with a weakened axial interaction, must be due to the enhanced Cu−N(His) interaction.

Type-1 (T1) blue copper proteins (cupredoxins) are ubiquitous electron-transfer (ET)[1] agents that readily accommodate the metal ion in both the Cu^{II} or Cu^{I} oxidation states. These proteins are characterized by unique properties when compared with copper coordination inorganic compounds (*1*, *2*). This includes an intense ligand-to-metal charge transfer (LMCT) absorption at approximately 600 nm (with a weaker LMCT band at ∼450 nm), an unusually small hyperfine coupling constant in the g_z region of their electron paramagnetic resonance (EPR) spectra (*1*−*4*), and a high reduction potential (*2*). The phytocyanins are a subclass of the cupredoxins that are found in plants (*5*−*10*) and have themselves been divided into three main groups (9), the stellacyanins, the plantacyanins, and the uclacyanins. Crystal structures of phytocyanins (*7*, *8*, *10*−*12*) demonstrate that members of this subfamily possess a more open β-sandwich structure compared to other cupredoxins (see Figure 1), which is stabilized by a disulfide bridge close to the active site (*7*, *8*, *10*−*12*). The copper ion is strongly coordinated by the thiolate sulfur of a Cys residue and the imidazole nitrogens of two His residues, as in all other cupredoxins (*7*, *8*, *10*, *11*). The T1 copper sites of stellacyanins are unusual in that they possess an axial Gln ligand (see Figure 1) (*7*, *11*, *12*), whereas the plantacyanins (and probably also the uclacyanins) have the more customary Met in this position (*8*, *10*).

An intriguing feature of all phytocyanins studied to date is a transition that occurs at high pH and results in the oxidized protein changing color from blue to violet (*5*, *14*−*22*). The main visible absorption band shifts from ∼600 nm at neutral pH to ∼580 nm at pH 11 (*14*−*22*). The weaker electronic absorption band at lower wavelength also shifts from ∼450 to ∼440 nm upon increasing pH. For both bands, a pK_a of ∼10 is obtained for this so-called alkaline transition (*15*). The transition also influences the EPR, electron nuclear double resonance, and paramagnetic ^1H nuclear magnetic resonance (NMR) spectral properties of the protein and alters the active-site structure (*15*, *17*, *20*, *23*−*26*). The reduction potential is also influenced at high pH, and thus, the alkaline transition may play a physiological role by tuning ET reactivity (*17*, *18*, *24*). There is currently no crystal structure

† This work was partially supported by FIRB-MIUR (Project "Molecular Nanodevices"), PRIN-MIUR 2004 project, BBSRC (Grant 13/B16498 to C.D.), and COST D21 (WG D21/0011/01).

* To whom correspondence should be addressed. Telephone: +39-0761-357136. Fax: +39-0761-357179. E-mail: cannistr@unitus.it (S.C.); Telephone: +44-191-222-7127. Fax: +44-191-222-7424. E-mail: christopher.dennison@ncl.ac.uk (C.D.).

‡ Università della Tuscia.

§ University of Newcastle upon Tyne.

[1] Abbreviations: ET, electron transfer; UMC, umecyanin, the stellacyanin from horseradish root; STC, stellacyanin from *Rhus vernicifera*; CST, stellacyanin from *Cucumis sativus*; LMCT, ligand-to-metal charge transfer; EPR, electron paramagnetic resonance; NMR, nuclear magnetic resonance; UV−vis, ultraviolet−visible; WT, wild type; DLS, dynamic light scattering; RR, resonance Raman; ACF, intensity autocorrelation function; RT, room temperature; Ac, amicyanin; CBP, cucumber basic protein; NiR, nitrite reductase; Paz, pseudoazurin; Pc, plastocyanin; Az, azurin.

10.1021/bi051702+ CCC: $30.25
Published on Web 11/12/2005

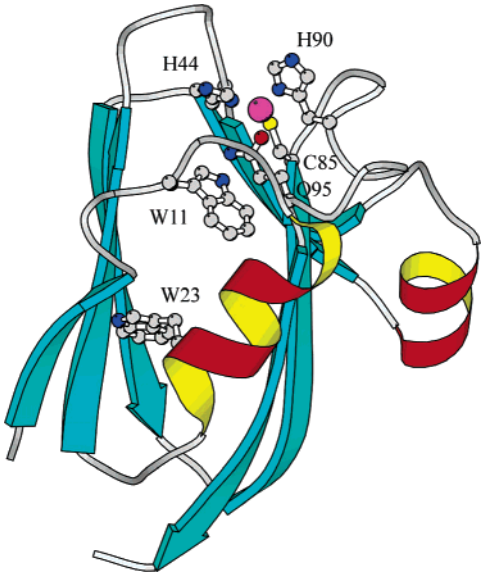

FIGURE 1: Structure of UMC (*11*) drawn with MOLSCRIPT (*13*) in which the Cu^{II} ion is shown in magenta and the side chains of the coordinating amino acids and also of Trp11 (~7 Å from the copper and involved in a π−amide interaction with the $N^{\epsilon}H_2$ moiety of the Gln ligand) and Trp23 (~15 Å from the copper) are included.

of a phytocyanin at high pH. Many studies have been devoted to the investigation of this phenomenon (*17*−*25*), and very recently, attention has focused on umecyanin (UMC), the stellacyanin from horseradish roots (*17*, *20*, *24*−*26*). A number of suggestions have been made for the cause of the alkaline transition, including a conserved Lys residue adjacent to the axial ligand (*17*), a change in the coordination mode of the axial Gln ligand in the stellacyanins (*23*, *27*), and a change in the secondary structure because of high molecular flexibility of the phytocyanins (*15*, *28*). The application of site-directed mutagenesis to the study of the cause of the alkaline transition in UMC has recently ruled out the axial Gln95 ligand and the conserved Lys as being responsible for this effect (*25*). All of these studies of the alkaline transition in the phytocyanins have failed to provide a conclusive answer as to its cause, and thus, a more comprehensive analysis of this phenomenon in a wild-type (WT) protein has been undertaken. This has included the use of resonance Raman (RR) spectroscopy, which provides detailed information about the copper site geometry of cupredoxins (*29*−*31*). Fluorescence spectroscopy has been used to investigate the environment of the Trp residues in UMC (Trp11 and Trp23), which should be very sensitive to subtle structural alterations (*32*) induced by the alkaline transition (Trp11 is involved in a π−amide interaction with the $N^{\epsilon}H_2$ moiety of the axial Gln ligand, and any active-site alterations would be expected to influence its fluorescence). It is reasonable to suppose that local geometrical changes could induce an overall reorganization of the protein, and to monitor this, we have analyzed the overall protein size during the alkaline transition using dynamic light scattering (DLS) (*33*).

MATERIALS AND METHODS

Materials. UMC was expressed in *Escherichia coli* and isolated and purified as described previously (*20*). For all optical measurements, UMC was exchanged into 20 mM Tris at pH 7.6. To vary the pH, small quantities of 100 mM solutions of NaOH and HCl were added to dilute UMC solutions. The final pH value of each sample was measured (Radiometer Copenhagen PHM82 Standard pH-meter). The concentration of protein samples was in the range of 30−60 μM, except for RR and DLS measurements, where the protein concentration was 0.86 mM.

Absorption Measurements. Absorption measurements were carried out at room temperature using a dual-beam ultraviolet−visible (UV−vis) spectrophotometer (Jasco V-550) in the spectral region of 200−800 nm with a 2.0 nm band-pass. For samples at pH 7.6, the UMC concentration was determined using $\epsilon_{606} = 4300\ M^{-1}\ cm^{-1}$ (*20*). For samples at pH values higher than 7.6, an estimated $\epsilon_{280} = 15\,500\ M^{-1}\ cm^{-1}$ was used. Measurements were carried out at a UMC concentration of 60 μM.

DLS Measurements. The DLS technique analyses temporal intensity fluctuations of the scattered light arising from particles diffusing in a well-defined volume (called scattering volume, that is the region of intersection of incident and scattered light and which depends upon the optical geometry) inside the investigated liquid sample (*33*). When fluctuations are principally determined by Brownian motion, the average diffusion coefficient of the scatterers can be obtained from the intensity autocorrelation function (ACF) of the scattered light, $g^2(t)$. This function represents the temporal correlation of the intensity of scattered light with itself. The mathematical description of ACF obtained for monomodal size distribution of spherical particles diffusing in a homogeneous liquid is

$$g^2(t) - 1 = \exp(-2\Gamma t) \tag{1}$$

where $\Gamma = 1/\tau = Dq^2$, $q = 4\pi n/\lambda \sin(\theta/2)$ is the scattering vector, τ is the characteristic time of the diffusion process, n is the index of refraction of the suspending medium, λ is the wavelength of the incident light, θ is the scattering angle, and D is the diffusion coefficient. In this hypothesis, D is given by the well-known Stokes−Einstein relation (eq 2)

$$D = \frac{k_B T}{3\pi\eta d} \tag{2}$$

where k_B is the Boltzmann constant, T is the absolute temperature, d is the hydrodynamic diameter of the scatterer, and η is the viscosity of the medium (*33*). At each pH, the solution viscosity has been determined using probe-DLS (*34*, *35*) by introducing a probe with known diameter inside the solution to measure the viscosity. The corresponding value of d was then determined by applying the Stokes−Einstein relation (eq 2). In all experiments, a $\theta = 90°$ scattering geometry and an Ar laser light source (Ion Laser Technology Inc.) running at 488 nm and 80 mW power have been used. The scattered light was detected by a photomultiplier and then passed to a BI-9000 (Brookhaven Instruments) digital correlator. All of the measurements have been performed at 25.0 ± 0.5 °C using filtered samples (0.22 μm, Millipore) to avoid the presence of dust.

Fluorescence Measurements. Fluorescence emission spectra have been collected at room temperature using a Spex Fluoromax spectrophotometer. The excitation wavelength for the emission spectra was 295 nm (band-pass of 3.0 nm) to minimize the signal from Tyr residues. The investigated

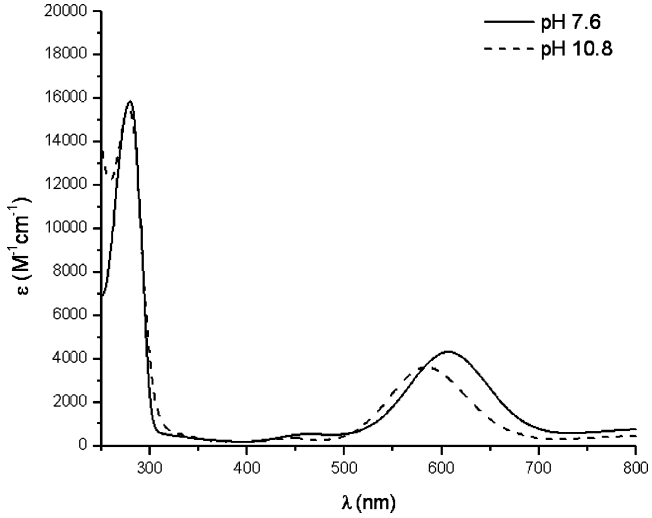

FIGURE 2: UV−vis spectra (25 °C) of Cu^{II} UMC in 20 mM Tris at pH 7.6 and 10.8.

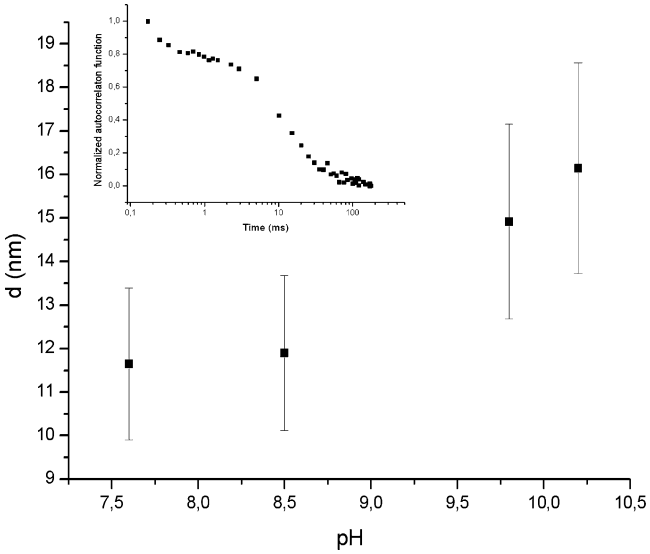

FIGURE 3: Dependence on pH of the protein diameter (*d*) extracted from the ACF parameters. A typical experimental ACF is shown in the inset.

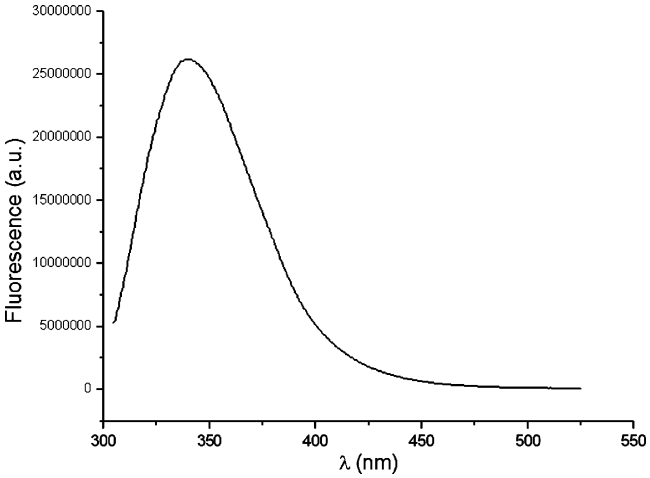

FIGURE 4: Emission spectrum of Cu^{II} UMC at pH 7.6 using an excitation wavelength of 295 nm.

emission region was 305−525 nm (emission band-pass of 5.0 nm). All spectra were corrected for the Raman signal of water and for auto-absorption and concentration effects. Measurements have been carried out at a Cu^{II} UMC concentration of 30 μM.

RR Measurements. RR spectra of a 0.86 mM UMC solution at two pH values (7.6 and 10.5) have been investigated using a Jobin Yvon LabRam confocal system equipped with a HeNe laser (633 nm, well inside the 600 nm absorption band of Cu^{II} UMC), and a 1800 gr/mm grating has been employed for measurements. The spectra reported have been acquired collecting the light, with a 40 mm objective, reflected from a quartz cuvette that contained the liquid sample. The laser power was 4 mW, and the system has a spectral resolution of ∼5 cm^{-1} and a data point increment of 1 cm^{-1} in the 200−1100 cm^{-1} region. To investigate some specific RR features in more detail, measurements were also carried out over a smaller region of the spectrum (200−400 cm^{-1}) with higher resolution (∼2 cm^{-1}) and a lower data point increment (0.3 cm^{-1}).

RESULTS AND DISCUSSION

Absorption. The UV−vis spectra of Cu^{II} UMC at two different pH values are presented in Figure 2. The spectrum at pH 7.6 is characterized by a feature at around 280 nm (with a shoulder at 290 nm) and two LMCT bands at ∼460 nm (λ_1) and ∼606 nm (λ_2). At pH 7.6, the $\epsilon_{464}/\epsilon_{606}$ ratio is 0.12. As the pH increases, the features around 280 nm do not change, while the LMCT bands shift to shorter wavelength in agreement with previous studies (*17*, *20*). The relative intensity of the two LMCT bands is unaffected by the alkaline transition.

DLS. From DLS measurements on Cu^{II} UMC, experimental ACF values have been recorded and the hydrodynamic diameter has been obtained as a function of pH (see Figure 3). As the pH is raised, the hydrodynamic diameter of UMC increases by ∼50%. Upon lowering the pH, the hydrodynamic diameter decreases, thus confirming the reversibility of the alkaline transition (*17*, *20*, *25*). The increase of the overall size of UMC during the alkaline transition mimics the behavior of cytochrome *c* during its alkaline transition (*36*). In the case of cytochrome *c*, it has been shown that the alkaline transition results in a partially denatured state that is characterized by an increase in the hydrodynamic radius of the protein (this process is reversible), which is smaller than what is typically observed for complete denaturation (*37*). Therefore, our results suggest that the conversion of UMC from the "neutral" to the "alkaline" form does not involve denaturation or gross structural changes and allow us to exclude protein aggregation occurring at high pH. The DLS results do indicate slight alterations in the overall protein structure are induced by the alkaline transition in UMC.

Steady-State Fluorescence. The steady-state fluorescence emission spectrum of Cu^{II} UMC at pH 7.6 obtained with excitation at 295 nm is shown in Figure 4. At this excitation wavelength, the fluorescence emission is mainly due to Trp residues. The spectrum shows a large peak located at around 340 nm. The position of this maximum indicates that the fluorescence-accessible Trp residues in UMC (Trp11 and Trp23) are solvent-exposed [when a Trp residue is not solvent-exposed, it has an emission at around 308 nm (*32*)]. Increasing pH has a limited effect on the fluorescence spectrum of UMC as shown in Figure 5. This demonstrates

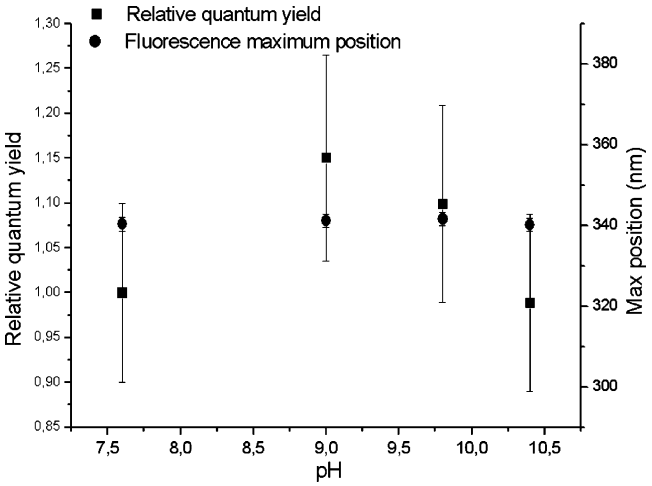

FIGURE 5: Relative quantum yield and the maximum position in the fluorescence emission spectrum of Cu^{II} UMC as a function of pH.

that the alkaline transition in UMC does not affect the microenvironment of either Trp11 or Trp23. This is particularly interesting for Trp11, which is involved in a π−amide interaction with the axial Gln95 ligand and has been considered as a cause of the alkaline transition (*25*). The results presented here highlight that the emitting Trp residues are not involved in the alkaline transition and that the alkaline transition does not have a dramatic effect on the overall active-site environment (which would be expected to influence Trp11).

RR. The RR spectra of Cu^{II} UMC at pH 7.6 and 10.5 in the spectral region 200−1100 cm^{-1} are shown in Figure 6. At pH 7.6, the RR spectrum of Cu^{II} UMC shows four intense peaks at 346, 386, 409, and 442 cm^{-1} and a shoulder at around 375 cm^{-1}, with the most intense peak being that at

Table 1: Resonance Raman Bands of UMC and Other Stellacyanins

STC[a]		UMC[b]		CST[c]	
RT	77 K	pH 7.6	pH 10.5	pH 5.5	pH 11.2
		267	269		
270	273			274	274
				281	283
	334 (sh)				
	347	346	345		
	359 (sh)			352	351
	374 (sh)	375	374	380	378
385	385	386	385	385	382
				396	396
405	405	409	407	411	409
422	422			420	420
	444	442	441	445	445
				482	482
750	746	742	744		

[a] Data for *Rhus vernicifera* stellacyanin obtained with 600 nm excitation (200 mW power) at room temperature (RT) and 77 K (*38*). [b] Data from the present study at two pH values. [c] Data for *Cucumis sativus* stellacyanin using 568 nm excitation (160 mW power) at 77 K and two pH values (*21*).

386 cm^{-1}. At lower frequency, a peak at 267 cm^{-1} is detected. A well-defined signal at 742 cm^{-1} is superimposed on a cluster of bands observed near 800 cm^{-1}. The comparison of this spectrum with those of other stellacyanins is reported in Table 1.

It is widely recognized that excitation of a cupredoxin within its S(Cys) → Cu^{II} LMCT band yields 4−12 fundamental vibrations in the 300−500-cm^{-1} region of the RR spectrum (*38*−*40*). The large number of frequencies compared to the single mode predicted for an isolated Cu−S center has been ascribed to kinematic and vibronic coupling of the Cu−S stretch with Cys ligand deformations (*38*). In particular, the strongest peak in the RR spectra of blue copper proteins results from a predominantly Cu−S(Cys) stretching

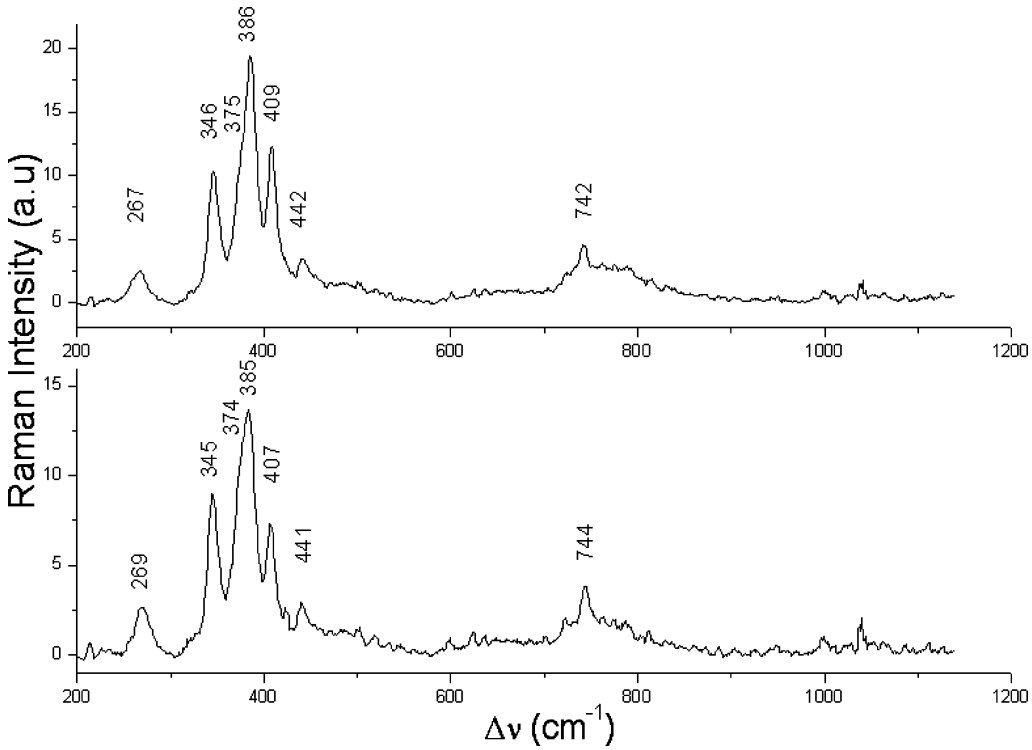

FIGURE 6: RR spectra of Cu^{II} UMC (at room temperature) at pH 7.6 (top) and 10.5 (bottom) using 633 nm excitation. Spectra have been obtained with an integration time of 60 s and with a 40 mm objective. The main peaks are labeled.

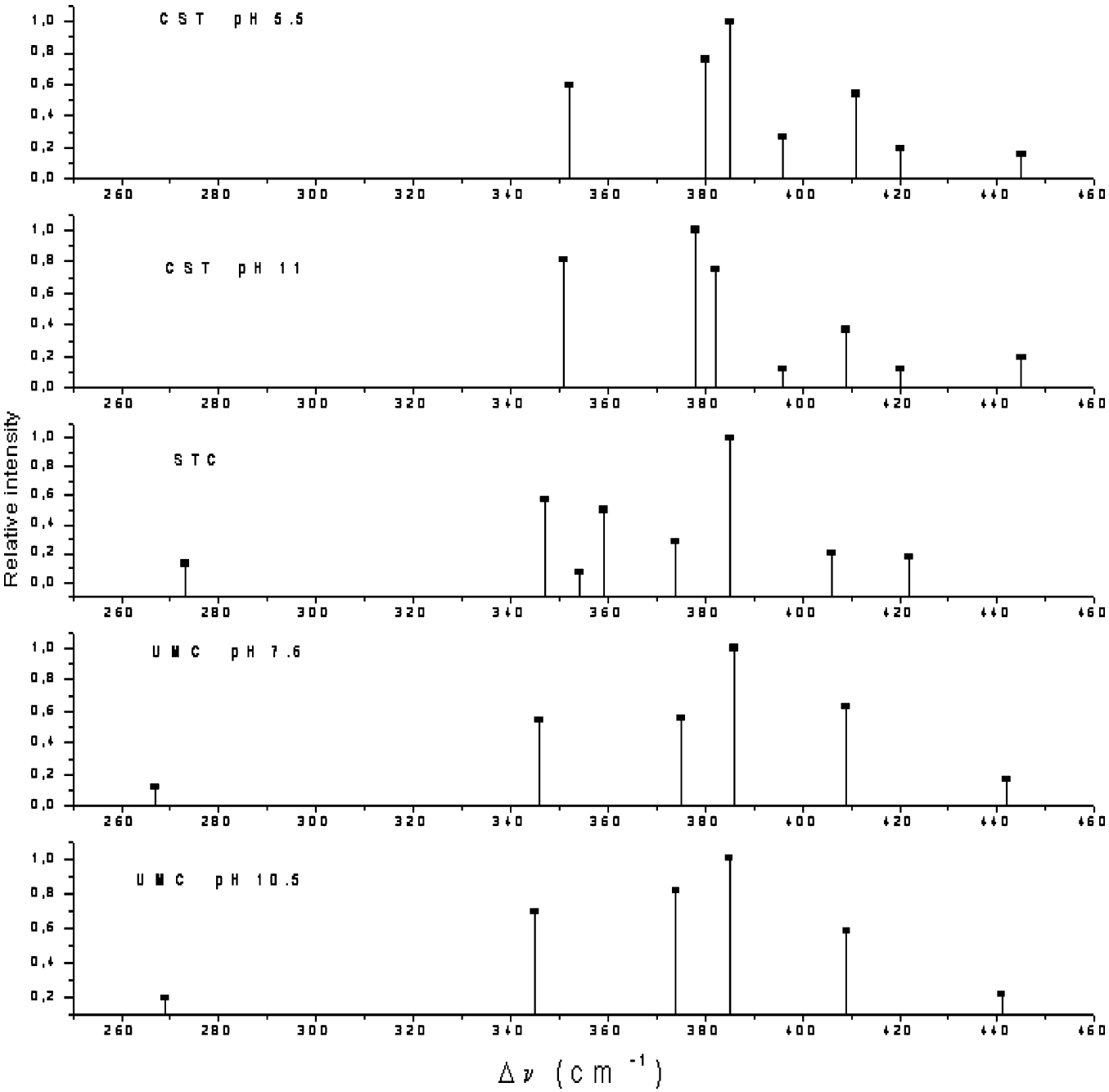

FIGURE 7: Relative intensities of peaks in the RR spectra of stellacyanins. The data for STC and CST are taken from refs *21* and *38*, respectively.

vibrational mode (*30*). The most intense peak in the spectrum of UMC occurs at 386 cm^{-1} (at pH 7.6), which has counterparts at almost identical positions in the spectra of *Rhus vernicifera* stellacyanin (STC) (*38*) and *Cucumis sativus* stellacyanin (CST) (*21*), suggesting that the Cu−S(Cys) bond strengths in these three proteins are very similar (see Figure 7). The positions of the other major peaks in the RR spectrum of UMC, arising from a combination of Cu−S and Cu−N stretching modes, are shifted by about 2−5 cm^{-1} compared to the analogous signals in CST and STC. In addition, the 409 cm^{-1} band has a counterpart in STC at 405 and 411 cm^{-1} in the spectrum of CST. The peak around 270 cm^{-1} in the spectra of blue copper proteins is usually assigned as a Cu−N(His) stretching vibration (*41*). In UMC, this band is located at 267 cm^{-1}, which is a lower frequency compared to its counterpart in STC (−3 cm^{-1}) and CST (−7 cm^{-1}).

In UMC, like other cupredoxins, the spectral region around 800 cm^{-1} possesses combination bands and overtones of the main peaks located in the 300−500 cm^{-1} region. This is usually associated with significant Duschinsky mixing of the excited state (*42*). The combination bands are generated by a principal band having the highest Cu−S character [ν_c Cu−S(Cys)] (*31*). The ν_c of 386 cm^{-1} for UMC allows us to quantitatively estimate a Cu^{II}−S(Cys) bond length of 2.15 Å using Badger's rule (*29*) [the change in bond distance, *r*, was calculated from the following relationship: $(r_1 - d_{ij})/(r_2 - d_{ij}) = (\nu_2/\nu_1)^{2/3}$, and for a bond between S and a first-row transition metal, d_{ij} was estimated to be 1.5] which is in good agreement with that observed in the crystal structure

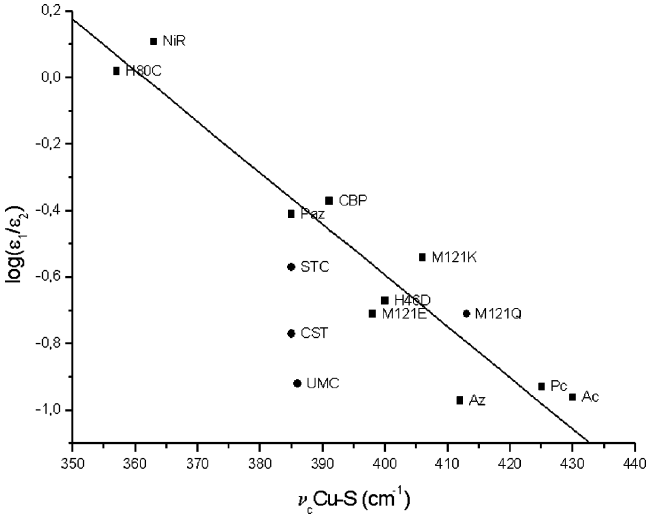

FIGURE 8: Correlation of the Cu−S(Cys) stretching frequency with the $\log(\epsilon_1/\epsilon_2)$ absorbance ratio for T1 Cu sites. Proteins included are amicyanin (Ac), azurin-H46D, SOD-Cu_2Cu_2-H80C (green), azurin-M121E (pH 3.9), azurin-Ml21K (pH 3.3), azurin-M121Q, cucumber basic protein (CBP), nitrite reductase (NiR), pseudoazurin (Paz), plastocyanin (Pc), STC, CST, and UMC. The ν_{Cu-S} in each case is ν_c; the frequency that generates the combination bands (*30*). The degree of T1 rhombicity decreases as $\log(\epsilon_1/\epsilon_2)$, and ν_c Cu−S increase. Cupredoxins having a Met as the axial ligand are indicated by ■, whereas cupredoxins having an axial Gln ligand are shown as ●. Data are taken from ref *30* and references therein, except for the data for UMC.

(2.2 ± 0.06 Å) (*11*). In the UMC spectrum, a well-defined band located at 742 cm^{-1}, assigned to a C−S stretch (*30*) of the Cys ligand, is detected.

There is a striking variability in the intensities of the different modes in cupredoxin RR spectra, and each class of protein has its own characteristic intensity pattern (*30*). To better understand this aspect of the spectra, we have compared the intensity of the RR patterns of selected stellacyanins in Figure 7. Vibrational intensities are related to the change in the geometry of the chromophore in the electronic excited state (*39*) and to differences in amino acid composition and protein structure in the vicinity of the blue copper site (but beyond the highly conserved His_2Cys equatorial ligand set). Han et al. (*39*) have proposed that the conformation of the peptide loop connecting the Cys and His ligands has an effect on the enhancement of particular RR modes in blue copper proteins. Thus, by comparing the intensity patterns shown in Figure 7, it appears that the structure in the vicinity of the active site of UMC is more similar to that in CST than STC.

A correlation between the intensity ratio of the LMCT bands in the UV−vis spectra of cupredoxins (ϵ_1/ϵ_2) and the main Cu−S(Cys) stretching vibration has been reported for cupredoxins (Figure 8) (*30*, *31*). T1 Cu sites with almost trigonal planar coordination (e.g., plastocyanin and amicyanin) have the highest ν_c Cu−S(Cys) values [and shortest Cu−S(Cys) bonds] and possess minimal absorbance at 460 nm in their UV−vis spectra (classic T1 sites). As T1 copper sites become more tetrahedral (going toward the T1 site of the green nitrite reductase), they exhibit lower ν_c Cu−S(Cys) RR frequencies [longer Cu−S(Cys) bonds] and increased absorbance at 460 nm relative to 600 nm (*31*) (distorted or perturbed T1 sites). At variance, the stellacyanins show an almost constant value for ν_c Cu−S(Cys) (see Figure 8). This could be representative of peculiar coordination geometries in the stellacyanins as a consequence of an axial Gln ligand, which may be related to the strength of this axial interaction and/or to the location of the amino acids within the Cu coordination sphere (*30*).

Table 2: Intensity-Weighted Average Frequency $\langle\nu_{Cu-S}\rangle$ of the Bands Associated with the Cu−S (Cys) Vibration in UMC and CST

protein	pH	$\langle\nu_{Cu-S}\rangle$ (cm^{-1})	protein	pH	$\langle\nu_{Cu-S}\rangle$ (cm^{-1})
UMC (RT)[a]	7.6	396	CST (77 K)[b]	5.5	388
UMC (RT)[a]	10.5	393	CST (77 K)[b]	11	382

[a] This study. [b] Calculated from the data reported in ref *21*.

Increasing the pH from 7.6 to 10.5 preserves the overall vibrational pattern in the RR spectrum of UMC. The 346, 375, 386, 409, and 442 cm^{-1} bands shift to lower frequency by ∼1−2 cm^{-1} at higher pH (Figure 6). This indicates that the Cu−S(Cys) bond length increases as a consequence of the alkaline transition. A similar effect is observed in the RR spectrum of CST at elevated pH (see Table 1 and Figure 7), but there are some variations. In particular, the shoulder of the 385 cm^{-1} peak located around 375 cm^{-1} increases in intensity with respect to the main peak in UMC, whereas in CST, the 375 cm^{-1} peak becomes even more intense than the one located at 385 cm^{-1} at high pH (see Figure 7). To circumvent the difficulties related to the definition of a peak position in the complex envelop of bands centered at ∼400 cm^{-1}, the intensity-weighted average $\langle\nu_{Cu-S}\rangle$ (eq 3) can be used (*43*)

$$\langle\nu_{Cu-S}\rangle = \frac{\sum_{\nu_i = 300\ cm^{-1}}^{500\ cm^{-1}} I_{\nu_i}\nu_i^2}{\sum_{\nu_i = 300\ cm^{-1}}^{500\ cm^{-1}} I_{\nu_i}\nu_i} \quad (3)$$

The $\langle\nu_{Cu-S}\rangle$ is indicative of the strength of the Cu−S(Cys) bond, and values for UMC are listed in Table 2 along with those extracted from published spectra for CST (*21*). The $\langle\nu_{Cu-S}\rangle$ values for UMC indicate a weakening of the Cu−S(Cys) bond upon increasing pH in agreement with the results of the single line analysis studies, and the same qualitative trend is found for CST. These findings are consistent with the results of paramagnetic NMR studies, which have demonstrated that the alkaline transition induces changes in the Cu active site resulting in a decreased Cu−S(Cys) interaction (*17*, *24*, *26*). It has also been found that the alkaline transition results in a weakening of the axial interaction in phytocyanins regardless of whether this residue is a Gln (as in the stellacyanins) or a Met (plantacyanins and uclacyanins) (*25*).

We also observe changes in the low-frequency region (100−300 cm^{-1}) of the RR spectrum of UMC as the pH increases. The feature at 267 cm^{-1} shifts to 269 cm^{-1} and becomes more intense at alkaline pH. Because the bands located in this region in the RR spectra of blue copper proteins arise from the Cu−N(His) stretch (*41*), these results indicate a shorter Cu^{II}−N(His) bond in the high pH form of UMC. Additional RR spectra have been acquired over a smaller region (200−400 cm^{-1}) with enhanced resolution

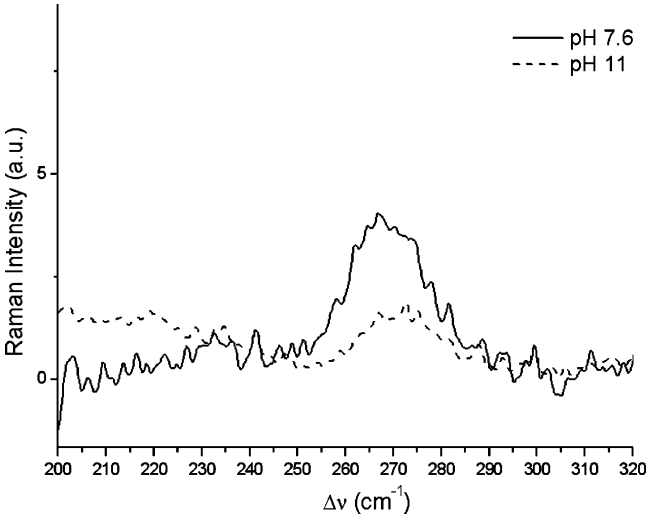

FIGURE 9: Detailed RR spectra of Cu^{II} UMC in the region of the Cu−N(His) stretching vibrations.

(Figure 9). The results of these studies show that the Cu−N(His) stretching vibration is shifted by 3.0 cm^{-1} to higher energy when the pH increases from 7.6 to 11. Thus, we can confirm that the alkaline transition induces a strengthening of the Cu−N(His) bond. It has been suggested recently that the deprotonation of the $N^{\epsilon 2}H$ moiety of one of the His ligands is the most likely cause of the alkaline transition (*25*). Deprotonation of a coordinated His will strengthen the bond that it makes with Cu^{II}, and our RR results provide direct experimental evidence for this. The strengthening of the interaction with the His ligand explains why the Cu^{II}−S(Cys) and Cu^{II}−S(Met) bonds are weakened at alkaline pH. The conclusion that deprotonation of one of the His ligands is the cause of the alkaline transition in the phytocyanins is also consistent with a very similar effect seen at high pH in rusticyanin (a cupredoxin but not a phytocyanin), which has been assigned to the deprotonation of the $N^{\epsilon 2}H$ of its exposed His143 ligand (*44*, *45*).

In summary, the studies reported herein demonstrate that the alkaline transition induces a slight reorganization of the structure of UMC and that the overall size of the protein increases, but that protein denaturation and aggregation do not occur. As a consequence of the alkaline transition, there are subtle alterations in the Cu site geometry. Direct evidence for the strengthening of a Cu−N(His) bond has been found, which is in agreement with the hypothesis that the deprotonation of the $N^{\epsilon 2}H$ moiety of one of the His ligands is the cause of the alkaline transition. A weakening of the Cu−S(Cys) bond has also been found, which, along with a weakened axial interaction, must be due to the enhanced Cu−N(His) interaction.

REFERENCES

1. Canters, G. W., and Gilardi, G. (1993) Engineering type 1 copper sites in proteins, *FEBS Lett. 325*, 39−48.
2. Solomon, E. I., Penfield, K. W., Gewirth, A. A., Lowery, M. D., Shadle, S. E., Guckert, J. A., and LaCroix, L. B. (1996) Electronic structure of the oxidized and reduced blue copper sites: Contributions to the electron-transfer pathway, reduction potential, and geometry, *Inorg. Chim. Acta 243*, 67−78.
3. Solomon, E. I., Baldwin, M. J., and Lowery, M. D. (1992) Electronic structures of active sites in copper proteins: Contributions to reactivity, *Chem. Rev. 92*, 521−542.
4. Guzzi, R., Bizzarri, A. R., Sportelli, L., and Cannistraro, S. (1997) An EPR investigation the structural heterogeneity in copper azurin and plastocyanin, *Biophys. Chem. 63*, 211−219.
5. Peisach, J., Levine, W. G., and Blumberg, W. E. (1967) Structural properties of stellacyanin, a copper mucoprotein from *Rhus vernicifera*, the Japanese lac tree, *J. Biol. Chem. 242*, 2847−2858.
6. van Driessche, G., Dennison, C., Sykes, A. G., and van Beeumen, J. (1995) Heterogeneity of the covalent structure of the blue copper protein umecyanin from horseradish roots, *Protein Sci. 4*, 209−227.
7. Hart, P. J., Nersissian, A. M., Herrmann, R. G., Nalbandyan, R. M., Valentine, J. S., and Eisenberg, D. (1996) A missing link in cupredoxins: Crystal structure of cucumber stellacyanin at 1.6 Å resolution, *Protein Sci. 5*, 2175−2183.
8. Guss, J. M., Merritt, E. A., Phizackerely, R. P., and Freeman, H. C. (1996) The structure of a phytocyanin, the basic blue protein from cucumber, refined at 1.8 Å resolution, *J. Mol. Biol. 262*, 686−705.
9. Nersissian, A. M., Immoos, C., Hill, M. G., Hart, P. J., Williams, G., Herrmann, R. G., and Valentine, J. S. (1998) Uclacyanins, stellacyanins, and plantacyanins are distinct subfamilies of phytocyanins: Plant-specific mononuclear blue copper proteins, *Protein Sci. 7*, 1915−1929.
10. Einsle, O., Mehrabian, Z., Nalbandyan, R., and Messerschmidt, A. (2000) Crystal structure of plantacyanin, a basic blue cupredoxin from spinach, *J. Biol. Inorg. Chem. 5*, 666−672.
11. Koch, M., Velarde, M., Harrison, M. D., Echt, S., Fischer, M., Messerschmidt, A., and Dennison, C. (2005) Crystal structures of oxidized and reduced stellacyanin from horseradish roots, *J. Am. Chem. Soc. 127*, 158−166.
12. Xie, Y., Inoue, T., Miyamoto, Y., Matsumura, H., Kataoka, K., Yamaguchi, K., Nojini, M., Suzuki, S., and Kai, Y. (2005) Structural reorganization of the copper binding site involving Thr^{15} of mavicyanin from *Cucurbita pepo medullosa* (zucchini) upon reduction, *J. Biochem. 137*, 455−461.
13. Kraulis, P. J. (1991) MOLSCRIPT−A program to produce both detailed and schematic plots of protein structures, *J. Appl. Crystallogr. 24*, 946−950.
14. Sakurai, T., Okamoto, H., Kawahara, K., and Nakahara, A. (1982) Some properties of a blue copper protein "plantacyanin" from cucumber peel, *FEBS Lett. 147*, 220−224.
15. Fernández, C. O., Sannazzaro, A. I., and Vila, A. J. (1997) Alkaline transition of *Rhus vernicifera* stellacyanin, an unusual blue copper protein, *Biochemistry 36*, 10566−10570.
16. De Kerpel, J. O. A., Pierloot, K., Ryde, U., and Roos, B. O. (1998) Theoretical study of the structural and spectroscopic properties of stellacyanin, *J. Phys. Chem. B 102*, 4638−4647.
17. Dennison, C., and Lawler, A. T. (2001) Investigation of the alkaline and acid transitions of umecyanin, a stellacyanin from horseradish roots, *Biochemistry 40*, 3158−3166.
18. Battistuzzi, G., Borsari, M., Loschi, L., Ranieri, A., Sola, M., Mondovi, B., and Marchesini, A. (2001) Redox properties and acid−base equilibria of zucchini mavicyanin, *J. Inorg. Biochem. 83*, 223−227.
19. Maritano, S., Marchesini, A., and Suzuki, S. (1997) Spectroscopic characterization of native and Co^{II}-substituted zucchini mavicyanin, *J. Biol. Inorg. Chem. 2*, 177−181.
20. Harrison, M. D., and Dennison, C. (2004) Characterization of *Arabidopsis thaliana* stellacyanin: A comparison with umecyanin, *Proteins 55*, 426−435.
21. Nersissian, A. M., Mehrabian, Z. B., Nalbandyan, R. M., Hart, P. J., Fraczkiewicz, G., Czernuszewicz, R. S., Bender, C. J., Peisach, J., Herrmann, R. G., and Valentine, J. S. (1996) Cloning, expression, and spectroscopic characterization of *Cucumis sativus* stellacyanin in its nonglycosylated form, *Protein Sci. 5*, 2184−2192.
22. Nersissian, A. M., and Nalbandyan, R. M. (1988) Studies on plantacyanin. III. Structural data obtained by CD and MCD methods and antigenic properties of the protein, *Biochim. Biophys. Acta 957*, 446−453.
23. Thomann, H., Bernardo, M., Baldwin, M. J., Lowery, M. D., and Solomon, E. I. (1991) Pulsed ENDOR study of the native and high pH perturbed forms of the blue copper site in stellacyanin, *J. Am. Chem. Soc. 113*, 5911−5913.
24. Dennison, C., Harrison, M. D., and Lawler, A. T. (2003) Alkaline transition of phytocyanins: A comparison of stellacyanin and umecyanin, *Biochem. J. 371*, 377−383.

25. Harrison, M. D., Yanagisawa, S., and Dennison, C. (2005) Investigating the cause of the alkaline transition of phytocyanins, *Biochemistry 44*, 3056−3064.
26. Dennison, C., and Harrison, M. D. (2004) The active-site structure of umecyanin, the stellacyanin from horseradish roots, *J. Am. Chem. Soc. 126*, 2481−2489.
27. Fields, B. A., Guss, J. M., and Freeman, H. C. (1991) Three-dimensional model for stellacyanin, a "blue" copper-protein, *J. Mol. Biol. 222*, 1053−1065.
28. Nersissian, A. M., Hart, P. J., and Valentine, J. S. (2000) Stellacyanin, a member of the phytocyanin family of plant proteins, in *Handbook of Metalloproteins* (Messerschmidt, A., Huber, R., Poulos, T., and Weighardt, K., Eds.) pp 1219−1234, John Wiley and Sons, Chichester, U.K.
29. Herschbach, D. R., and Laurie, V. W. (1961) Anharmonic potential constants and their dependence on bond length, *J. Chem. Phys. 35*, 458−464.
30. Andrew, C. R., Yeom, H., Valentine, J. S., Karlsson, B. G., Bonander, N., van Pouderoyen, G., Canters, G. W., Loehr, T. M., and Sanders-Loehr, J. (1994) Raman spectroscopy as an indicator of Cu−S bond length in type 1 and type 2 copper cysteinate proteins, *J. Am. Chem. Soc. 116*, 11489−11498.
31. Andrew, C. R., and Sanders-Loehr, J. (1996) Copper−sulfur proteins: Using Raman spectroscopy to predict coordination geometry, *Acc. Chem. Res. 29*, 365−372.
32. Lakowicz, J. R., Ed. (1991) *Topics in Fluorescence Spectroscopy*, Vol. 3, pp 113−136, Plenum Press, New York.
33. Berne, B. J., and Pecora, R. (1976) *Dynamic Light Scattering with Applications to Chemistry, Biology, and Physics*, pp 3−52, Wiley-Interscience, New York.
34. Placidi, M., and Cannistraro, S. (1998) A dynamic light scattering study on mutual diffusion coefficient of BSA in concentrated aqueous solutions, *Europhys. Lett. 43*, 476−481.
35. Delfino, I., Piccolo, C., and Lepore, M. (2005) Experimental study of short- and long-time diffusion regimes of spherical particles in carboxymethylcellulose solutions, *Eur. Pol. J. 41*, 1772−1780.
36. Bonincontro, A., and Risuleo, G. (2003) Dielectric spectroscopy as a probe for the investigation of conformational properties of proteins, *Spectrochim. Acta, Part A 59*, 2677−2684.
37. Weber, C., Michel, B., and Bosshard, H. R. (1987) Spectroscopic analysis of the cytochrome *c* oxidase−cytochrome *c* complex: Circular dichroism and magnetic circular dichroism measurements reveal change of cytochrome *c* heme geometry imposed by complex formation, *Proc. Natl. Acad. Sci. U.S.A. 84*, 6687−6691.
38. Nestor, L., Larrabee, J. A., Woolery, G., Reinhammar, B., and Spiro, T. G. (1984) Resonance Raman spectra of blue copper proteins: Assignments from normal mode calculations and copper-63/copper-65 and H_2O/D_2O shifts for stellacyanin and laccase, *Biochemistry 23*, 1084−1093.
39. Han, J., Adman, E. T., Beppu, T., Codd, R., Freeman, H. C., Huq, L., Loehr, T. M., and Sanders-Loehr, J. (1991) Resonance Raman spectra of plastocyanin and pseudoazurin: Evidence for conserved cysteine ligand conformations in cupredoxins (blue copper proteins), *Biochemistry 30*, 10904−10913.
40. Bizzarri, A. R., and Cannistraro, S. (2001) Intensity fluctuations of the copper site resonant vibrational modes as studied by MD simulation in single plastocyanin molecule, *Chem. Phys. Lett. 349*, 503−510.
41. Dave, B. C., Germanas, J. P., and Czernuszewicz, R. S. (1993) The first direct evidence for copper(II)−cysteine vibrations in blue copper proteins: Resonance Raman spectra of ^{34}S-Cys-labeled azurins reveal correlation of copper−sulfur stretching frequency with metal site geometry, *J. Am. Chem. Soc. 115*, 12175−12176.
42. Blair, D. F., Campbell, G. W., Schoonover, J. R., Chan, S. I., Gray, H. B., Malmström, B. G., Pecht, I., Swanson, B. I., Woodruff, W. H., Cho, W. K., English, A. M., Fry, H. A., Lum, V., and Norton, K. A. (1985) Resonance Raman studies of blue copper proteins: Effect of temperature and isotopic substitutions. Structural and thermodynamic implications, *J. Am. Chem. Soc. 107*, 5755−5766.
43. Basumallick, L., Szilagyi, R. K., Zhao, Y., Shapleigh, J. P., Scholes, C. P., and Solomon, E. I. (2003) Spectroscopic studies of the Met182Thr mutant of nitrite reductase: Role of the axial ligand in the geometric and electronic structure of blue and green copper sites, *J. Am. Chem. Soc. 125*, 14784−14792.
44. Nunzi, F., Guerlesquin, F., Shepard, W., Guigliarelli, B., and Bruschi, M. (1994) Active site geometry in the high oxido-reduction potential rusticyanin from *Thiobacillus ferrooxidans*, *Biochem. Biophys. Res. Commun. 203*, 1655−1662.
45. Giudici-Orticoni, M. T., Guerlesquin, F., Bruschi, M., and Nitschke, W. (1999) Interaction-induced redox switch in the electron-transfer complex rusticyanin−cytochrome c_4, *J. Biol. Chem. 274*, 30365−30369.

BI051702+